nature genetics

Lis1 regulates asymmetric division in hematopoietic stem cells and in leukemia

Bryan Zimdahl[1–3,12], Takahiro Ito[1,2,12], Allen Blevins[1,2], Jeevisha Bajaj[1,2], Takaaki Konuma[1,2], Joi Weeks[1,2], Claire S Koechlein[1,2], Hyog Young Kwon[1,2], Omead Arami[1,2], David Rizzieri[4], H Elizabeth Broome[5,6], Charles Chuah[7,8], Vivian G Oehler[9], Roman Sasik[10], Gary Hardiman[10,11] & Tannishtha Reya[1–3,6]

Cell fate can be controlled through asymmetric division and segregation of protein determinants, but the regulation of this process in the hematopoietic system is poorly understood. Here we show that the dynein-binding protein Lis1 is critically required for hematopoietic stem cell function and leukemogenesis. Conditional deletion of *Lis1* (also known as *Pafah1b1*) in the hematopoietic system led to a severe bloodless phenotype, depletion of the stem cell pool and embryonic lethality. Further, real-time imaging revealed that loss of *Lis1* caused defects in spindle positioning and inheritance of cell fate determinants, triggering accelerated differentiation. Finally, deletion of *Lis1* blocked the propagation of myeloid leukemia and led to a marked improvement in survival, suggesting that Lis1 is also required for oncogenic growth. These data identify a key role for Lis1 in hematopoietic stem cells and mark its directed control of asymmetric division as a critical regulator of normal and malignant hematopoietic development.

A key question in biology is how cell fate decisions are regulated and how disruption of this regulation can lead to cancer. One fundamental mechanism that controls fate is asymmetric cell division, which involves the polarized distribution of determinants within the mother cell and their unequal inheritance by each daughter cell. Such asymmetric division allows one daughter cell to become differentiated and the other to retain an immature fate; in contrast, symmetric division allows both daughter cells to adopt equivalent fates. Studies in invertebrates such as *Drosophila melanogaster* have elucidated the major steps involved in asymmetric cell division, which include the establishment of polarity, localization of fate determinants and orientation of the mitotic spindle. A key regulator of this process is Lis1, a dynein-binding protein that anchors the mitotic spindle to the cellular cortex[1,2]. By determining the orientation of the spindle, Lis1 ensures that the proper cleavage plane is established during cell division, thus allowing correct inheritance of fate determinants by daughter cells.

Whereas the regulation of asymmetric cell division in invertebrates is well understood, relatively little is known about how it influences hematopoietic development, and even less is known about its role in malignancy. Previous work from our laboratory and others has shown that hematopoietic stem and progenitor cells can undergo both symmetric and asymmetric division[3–5]. These findings were supported by more recent studies indicating that genetic modulation of fate determinants[4,6–10] can affect hematopoietic stem cell (HSC) function. But how inheritance of fate determinants is controlled during asymmetric division and whether disruption of this process can affect hematopoietic cell fate and tumorigenesis *in vivo* remain unknown. Here we have addressed these questions by focusing on Lis1, and we show that its genetic loss triggers an inability to maintain the stem cell state in both normal and malignant hematopoiesis. Conditional deletion of *Lis1* in hematopoietic cells leads to a dramatic 'bloodless' phenotype, impaired stem cell function and depletion of the stem cell pool. Mechanistically, loss of *Lis1* in stem cells does not seem to influence proliferation or apoptosis but leads to accelerated differentiation. At a molecular level, fate determinants such as Numb are properly polarized, but their inheritance is impaired, with more frequent segregation to one daughter cell driving an increase in the frequency of asymmetric divisions. We also examined the role of Lis1 in cancer to gain a better understanding of whether and how asymmetric division controls oncogenesis and to define new signals that may be targeted by therapy. Using mouse models and human samples of aggressive leukemias, we found that Lis1 is critical for the growth and propagation of blast-crisis chronic myelogenous leukemia (CML) and therapy-resistant *de novo* acute myelogenous leukemia (AML). These data show that Lis1 has a crucial role in the establishment of the hematopoietic system and controls normal and malignant stem cell function.

[1]Department of Pharmacology, University of California San Diego School of Medicine, La Jolla, California, USA. [2]Sanford Consortium for Regenerative Medicine, La Jolla, California, USA. [3]Department of Pharmacology and Cancer Biology, Duke University Medical Center, Durham, North Carolina, USA. [4]Division of Cell Therapy, Department of Medicine, Duke University Medical Center, Durham, North Carolina, USA. [5]Department of Pathology, University of California San Diego School of Medicine, La Jolla, California, USA. [6]Moores Cancer Center, University of California San Diego School of Medicine, La Jolla, California, USA. [7]Department of Haematology, Singapore General Hospital, Singapore. [8]Cancer and Stem Cell Biology Program, Duke–National University of Singapore Graduate Medical School, Singapore. [9]Clinical Research Division, Fred Hutchinson Cancer Research Center, Seattle, Washington, USA. [10]Department of Medicine, University of California San Diego School of Medicine, La Jolla, California, USA. [11]Computational Science Research Center and Biomedical Informatics Research Center, San Diego State University, San Diego, California, USA. [12]These authors contributed equally to this work. Correspondence should be addressed to T.R. (treya@ucsd.edu).

Received 29 August 2013; accepted 9 January 2014; published online 2 February 2014; doi:10.1038/ng.2889

RESULTS

Loss of *Lis1* leads to a bloodless phenotype

To study the role of Lis1 in the hematopoietic system, we generated mice in which a *loxP*-flanked *Lis1* allele[11] was conditionally deleted by Cre recombinase whose expression was under the control of the *Vav1* promoter (*Lis1*$^{f/f}$; *Vav1-cre*)[12–14]. This approach led to loss of *Lis1* expression in hematopoietic cells and enabled assessment of the role of Lis1 in the establishment of the hematopoietic system (**Supplementary Fig. 1**). Of the 344 viable progeny obtained, none of the 86 expected *Lis1*-null mice were born. In a retrospective analysis, we found that loss of *Lis1* led to a striking bloodless phenotype, indicative of severe anemia, at embryonic day (E) 14.5 (**Fig. 1a**). Subsequently, loss of *Lis1* led to lethality between E15.5 and E18.5 (**Supplementary Table 1**). Histologically, *Lis1* deletion led to loss of hematopoietic cells (**Fig. 1a**) and a ~13.5-fold reduction in the frequency of HSCs (c-Kit$^+$Lin$^-$AA4.1$^+$ or KL AA4.1$^+$ cells; **Fig. 1b**) in the fetal liver. Notably, the sevenfold expansion in the HSC population that normally occurs between E12.5 and E15.5 and leads to the generation of a functional hematopoietic system (**Fig. 1c**, filled squares) did not occur in the absence of *Lis1* (**Fig. 1c**, open squares).

To determine whether the failure of HSC expansion *in vivo* was linked to functional defects in HSCs, we assessed colony formation in methylcellulose cultures. Loss of *Lis1* led to a threefold reduction in total colony formation; the fact that the colonies formed were similar for wild-type (*Lis1*$^{f/+}$ or *Lis1*$^{f/f}$) and *Lis1*-deficient cells indicates that differentiation potential was unaffected (**Fig. 1d** and **Supplementary Fig. 2**). Further, transplantation with wild-type (*Lis1*$^{f/+}$) HSC-enriched cells (Lin$^-$AA4.1$^+$) led to ~53% donor chimerism in recipient mice 4 months after transplantation, whereas no chimerism (0%) was detected in mice reconstituted with *Lis1*-deficient cells (**Fig. 1e**,**f**), suggesting that loss of *Lis1* affects fetal HSC function. Unsorted whole fetal liver transplants also showed loss of chimerism, indicating that *Lis1* deletion affected functional HSCs and is unlikely to have simply changed their phenotype (data not shown).

Lis1 is required for adult hematopoietic stem cell function

To determine whether Lis1 has a conserved functional role in the adult hematopoietic system, we crossed the mice with *loxP*-flanked *Lis1* to mice harboring a *cre-ER*^{T2} allele targeted to the ubiquitously expressed *Rosa26* locus[15] (*Lis1*$^{f/f}$; *Rosa26-creER*, denoted hereafter as *Lis1*$^{f/f}$; *creER* mice). Tamoxifen delivery allowed effective temporal control of *Lis1* deletion (**Supplementary Fig. 3a**,**b**) and a clear reduction in *Lis1* mRNA expression in adult bone marrow HSC-enriched cells (c-Kit$^+$Lin$^-$Sca1$^+$ or KLS cells; **Supplementary Fig. 3b**,**c**). Consistent with this observation, Lis1 protein expression was reduced in highly enriched HSCs (KLS CD48$^-$ cells; **Supplementary Fig. 3d**). Loss of *Lis1* led to a significant reduction in the frequency and absolute number of adult HSCs (**Fig. 2a**,**b** and **Supplementary Fig. 4**). HSC defects preceded any changes in differentiated cells, suggesting that HSC maintenance is directly affected by loss of Lis1 (**Supplementary Fig. 5**). Adult HSC function was also affected by the deletion of *Lis1*; whereas transplanted HSCs from control mice increased donor chimerism from 39 to 51%, mice reconstituted with *Lis1*-deficient cells showed a gradual loss of donor chimerism from ~6.5 to 0% (**Fig. 2c**,**d**). Genome-wide expression analysis of HSC-enriched cells from control and *Lis1*-null mice showed a highly significant loss of expression of the core genes that form the stem cell signature[16–18] (**Supplementary Fig. 6**), as well as changes in the expression of genes such as *Pim1* and *Socs3* that have important regulatory roles in hematopoietic stem and progenitor cell maintenance and differentiation (**Fig. 2e**). The fact that *Lis1* deletion triggers loss of the stem cell signature confirms that Lis1 is critical to maintenance of the stem cell state through an independent molecular strategy.

Because Cre expression was under the control of a ubiquitous promoter, it was possible that deletion of *Lis1* in non-hematopoietic tissues contributed to impaired maintenance of HSCs. To address this possibility, we created chimeras in which only hematopoietic cells harbored the *loxP*-flanked allele and the microenvironment remained wild type. HSCs from untreated control *Lis1*$^{+/+}$; *creER* or *Lis1*$^{f/f}$; *creER* mice were used for transplantation (**Supplementary Fig. 7**); following repopulation with donor cells (**Fig. 2f**), chimeras were treated with tamoxifen to delete *Lis1* specifically in the hematopoietic system. This deletion led to a marked reduction in the frequency of HSC-enriched cells (**Fig. 2g**). Donor-derived whole bone marrow from both control and *Lis1*-deficient chimeras was retransplanted to test stem cell function. Whereas the average chimerism from control cells was 53.5%, chimerism from *Lis1*-null cells was nearly absent (0.3%; **Fig. 2h**,**i**), roughly recapitulating the phenotype of non-chimeric

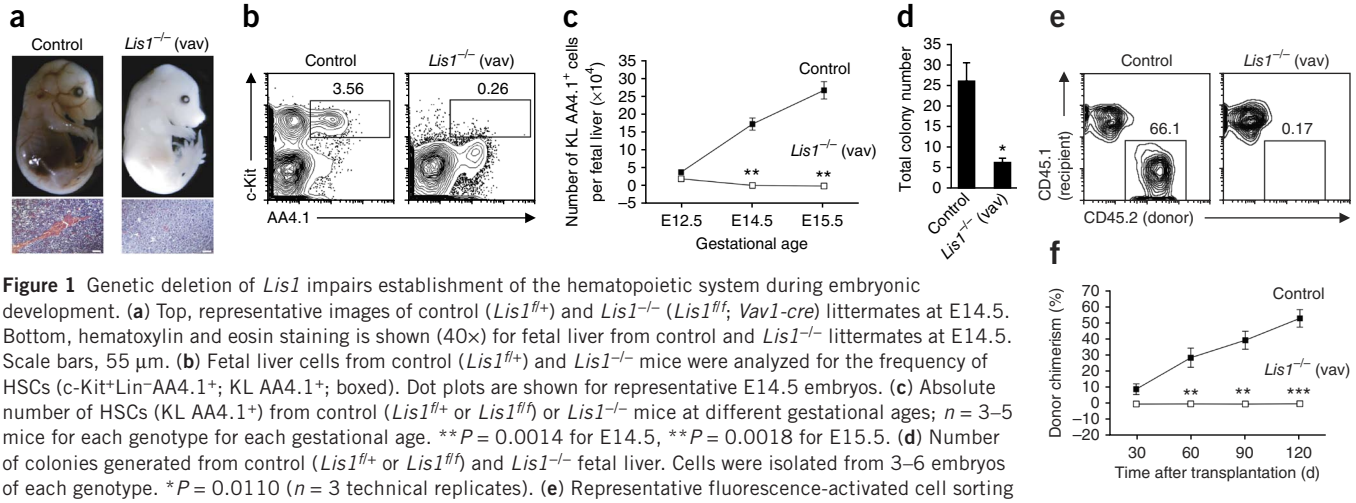

Figure 1 Genetic deletion of *Lis1* impairs establishment of the hematopoietic system during embryonic development. (**a**) Top, representative images of control (*Lis1*$^{f/+}$) and *Lis1*$^{-/-}$ (*Lis1*$^{f/f}$; *Vav1-cre*) littermates at E14.5. Bottom, hematoxylin and eosin staining is shown (40×) for fetal liver from control and *Lis1*$^{-/-}$ littermates at E14.5. Scale bars, 55 μm. (**b**) Fetal liver cells from control (*Lis1*$^{f/+}$) and *Lis1*$^{-/-}$ mice were analyzed for the frequency of HSCs (c-Kit$^+$Lin$^-$AA4.1$^+$; KL AA4.1$^+$; boxed). Dot plots are shown for representative E14.5 embryos. (**c**) Absolute number of HSCs (KL AA4.1$^+$) from control (*Lis1*$^{f/+}$ or *Lis1*$^{f/f}$) or *Lis1*$^{-/-}$ mice at different gestational ages; $n = 3$–5 mice for each genotype for each gestational age. $^{**}P = 0.0014$ for E14.5, $^{**}P = 0.0018$ for E15.5. (**d**) Number of colonies generated from control (*Lis1*$^{f/+}$ or *Lis1*$^{f/f}$) and *Lis1*$^{-/-}$ fetal liver. Cells were isolated from 3–6 embryos of each genotype. $^{*}P = 0.0110$ ($n = 3$ technical replicates). (**e**) Representative fluorescence-activated cell sorting (FACS) profiles of donor chimerism (4 months; boxed) in CD45.1$^+$ recipients transplanted with HSC-enriched cells (Lin$^-$AA4.1$^+$) from either control (*Lis1*$^{f/+}$) or *Lis1*$^{-/-}$ E14.5 embryos. (**f**) Average donor chimerism at different times after transplantation (2–4 donor mice were used for each genotype, and 4–6 recipient mice were included in each cohort). $^{**}P = 0.0088$ for 60 d, $^{**}P = 0.0021$ for 90 d, and $^{***}P = 0.0006$ for 120 d. All error bars, s.e.m.

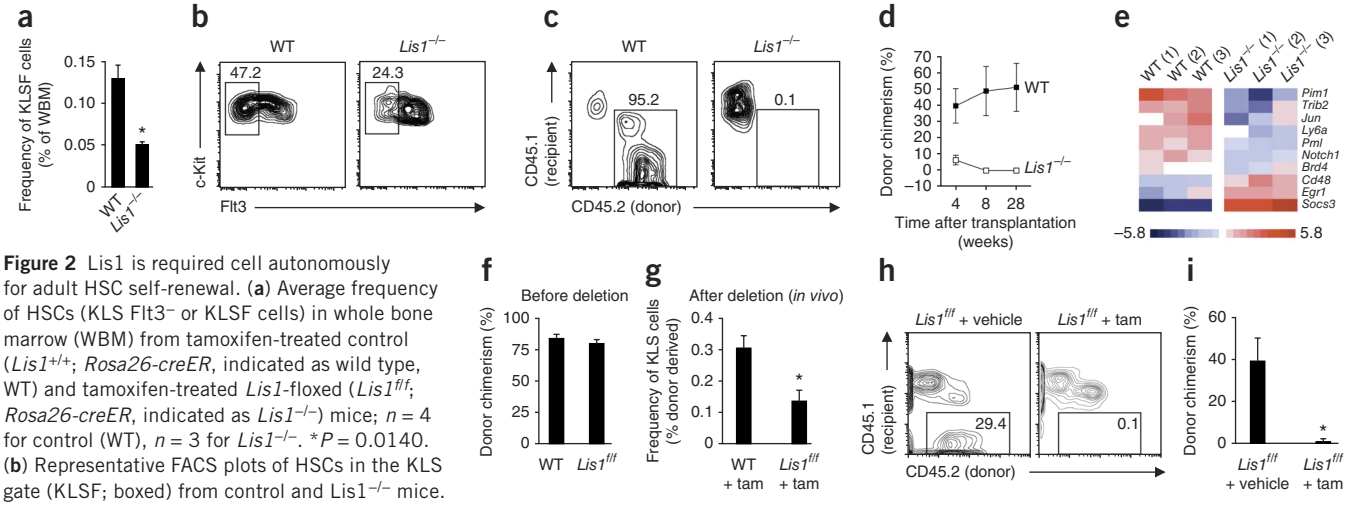

Figure 2 Lis1 is required cell autonomously for adult HSC self-renewal. (**a**) Average frequency of HSCs (KLS Flt3$^-$ or KLSF cells) in whole bone marrow (WBM) from tamoxifen-treated control (*Lis1*$^{+/+}$; *Rosa26-creER*, indicated as wild type, WT) and tamoxifen-treated *Lis1*-floxed (*Lis1*$^{f/f}$; *Rosa26-creER*, indicated as *Lis1*$^{-/-}$) mice; $n = 4$ for control (WT), $n = 3$ for *Lis1*$^{-/-}$. $^*P = 0.0140$. (**b**) Representative FACS plots of HSCs in the KLS gate (KLSF; boxed) from control and Lis1$^{-/-}$ mice. (**c**) Repopulation efficiency of *Lis1*$^{-/-}$ HSCs. Representative FACS plots show donor chimerism (CD45.2$^+$ cells; boxed) in recipients transplanted with HSCs (KLS CD150$^+$CD48$^-$) from control or *Lis1*$^{-/-}$ mice. FACS analysis was performed 28 weeks after transplantation. (**d**) Average donor chimerism at different times after transplantation (4–5 mice per cohort). (**e**) Genome-wide expression analysis of *Lis1*-deficient HSC-enriched cells. The heat map shows known regulators of stem and progenitor cell activity significantly affected by the loss of *Lis1* (false discovery rate (FDR) < 0.01). (**f**–**i**) *Lis1* chimeras with hematopoietic-specific *Lis1* deletion. (**f**) Donor chimerism before tamoxifen (tam) treatment was assessed 2 months after transplantation of mice with control (*Lis1*$^{+/+}$; *Rosa26-creER*, WT) or *Lis1*$^{f/f}$; *Rosa26-creER* (*Lis1*$^{f/f}$) HSCs ($n = 5$ mice in each cohort). (**g**) Frequency of donor-derived KLS cells in chimeric mice after deletion. "WT + tam" indicates mice that received donor cells from *Lis1*$^{+/+}$; *Rosa26-creER* mice, and "*Lis1*$^{f/f}$ + tam" indicates mice that received donor cells from *Lis1*$^{f/f}$; *Rosa26-creER* mice; $n = 3$ for each cohort. $^*P = 0.0277$. (**h**,**i**) Repopulation ability of whole bone marrow cells isolated from *Lis1* chimera mice. (**h**) Representative FACS plots show donor chimerism (CD45.2$^+$ cells; boxed) in recipients of cells from either controls (*Lis1*$^{f/f}$ + vehicle) or *Lis1* chimeras (*Lis1*$^{f/f}$ + tam). (**i**) Average donor chimerism 16 weeks after transplantation ($n = 3$–4 recipients per cohort. $^*P = 0.0369$). All error bars indicate the s.e.m.

Lis1-null mice. These data suggest that adult *Lis1*-deficient HSCs have a cell-autonomous functional defect *in vivo*.

Lis1 deletion impairs inheritance of fate determinants

To understand how stem cells are lost in the absence of Lis1, we first examined proliferation and apoptosis. *Lis1*-deficient HSCs (KLS CD150$^+$CD48$^-$), HSC-enriched cells (KLS) and multipotent precursors (KLS CD150$^-$CD48$^+$) incorporated 5-bromodeoxyuridine (BrdU) at a rate similar to that observed in equivalent cells from wild-type mice and displayed a normal cell cycle distribution (**Fig. 3a**–**c** and **Supplementary Fig. 8**). In contrast, differentiated cells showed decreased proliferation (data not shown), indicating that Lis1 may have context-specific effects at distinct stages of development, consistent with observations in the nervous system[2]. *Lis1*-deficient

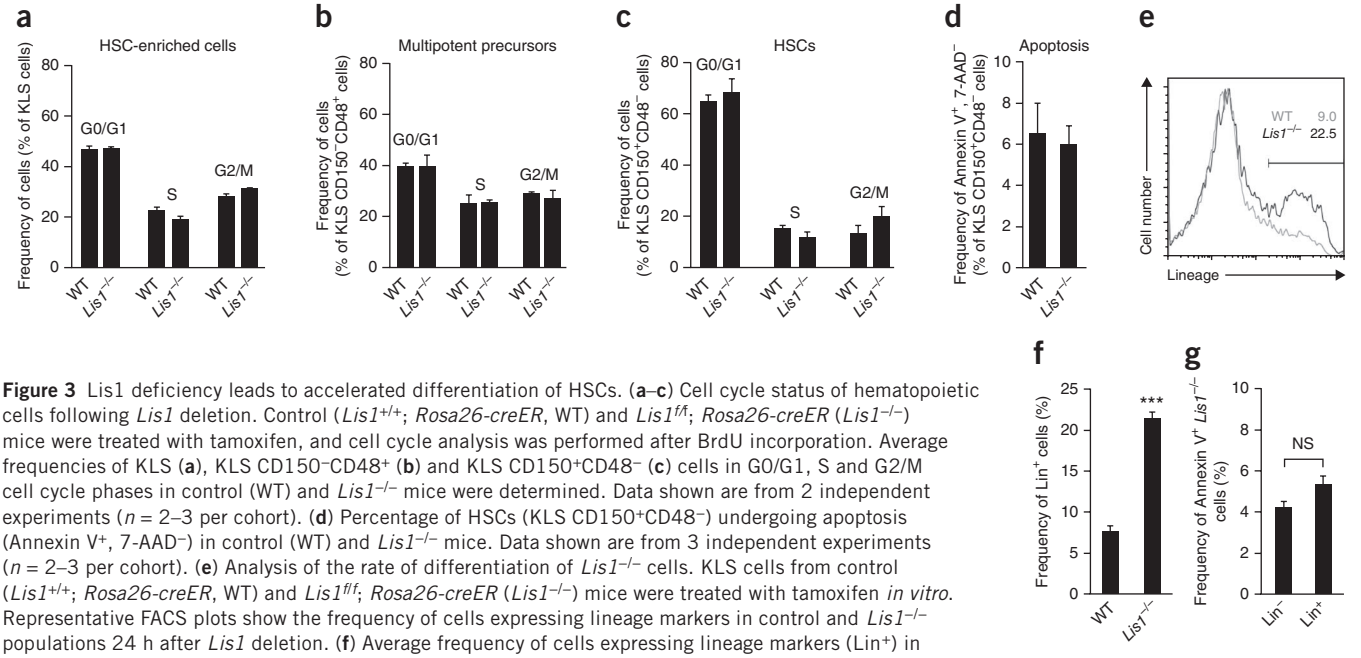

Figure 3 Lis1 deficiency leads to accelerated differentiation of HSCs. (**a**–**c**) Cell cycle status of hematopoietic cells following *Lis1* deletion. Control (*Lis1*$^{+/+}$; *Rosa26-creER*, WT) and *Lis1*$^{f/f}$; *Rosa26-creER* (*Lis1*$^{-/-}$) mice were treated with tamoxifen, and cell cycle analysis was performed after BrdU incorporation. Average frequencies of KLS (**a**), KLS CD150$^-$CD48$^+$ (**b**) and KLS CD150$^+$CD48$^-$ (**c**) cells in G0/G1, S and G2/M cell cycle phases in control (WT) and *Lis1*$^{-/-}$ mice were determined. Data shown are from 2 independent experiments ($n = 2$–3 per cohort). (**d**) Percentage of HSCs (KLS CD150$^+$CD48$^-$) undergoing apoptosis (Annexin V$^+$, 7-AAD$^-$) in control (WT) and *Lis1*$^{-/-}$ mice. Data shown are from 3 independent experiments ($n = 2$–3 per cohort). (**e**) Analysis of the rate of differentiation of *Lis1*$^{-/-}$ cells. KLS cells from control (*Lis1*$^{+/+}$; *Rosa26-creER*, WT) and *Lis1*$^{f/f}$; *Rosa26-creER* (*Lis1*$^{-/-}$) mice were treated with tamoxifen *in vitro*. Representative FACS plots show the frequency of cells expressing lineage markers in control and *Lis1*$^{-/-}$ populations 24 h after *Lis1* deletion. (**f**) Average frequency of cells expressing lineage markers (Lin$^+$) in control and *Lis1*$^{-/-}$ cells. Data shown are from three independent experiments (3 mice in each cohort). $^{***}P = 0.0002$. (**g**) Analysis of apoptosis in Lin$^-$ and Lin$^+$ fractions of *Lis1*$^{-/-}$ cells. Percentages of Annexin V$^+$ cells 24 h after *Lis1* deletion are shown. Data shown are from two independent experiments. NS, not significant. All error bars, s.e.m.

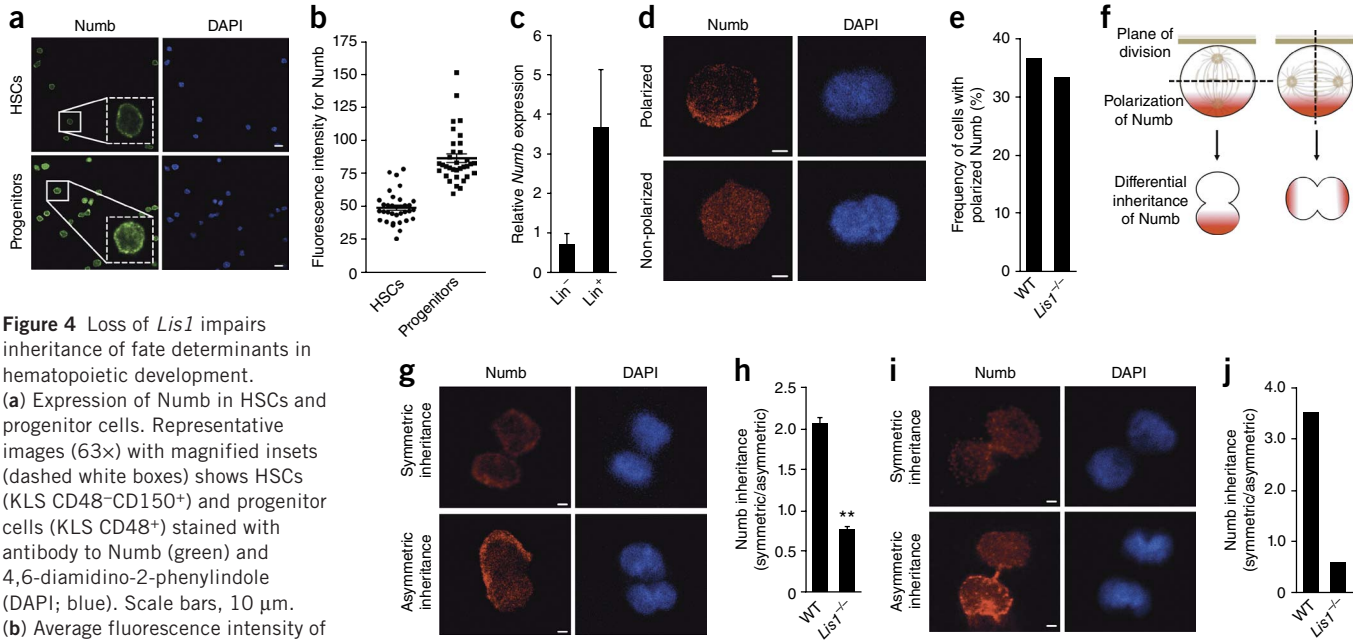

Figure 4 Loss of *Lis1* impairs inheritance of fate determinants in hematopoietic development. (**a**) Expression of Numb in HSCs and progenitor cells. Representative images (63×) with magnified insets (dashed white boxes) shows HSCs (KLS CD48$^-$CD150$^+$) and progenitor cells (KLS CD48$^+$) stained with antibody to Numb (green) and 4,6-diamidino-2-phenylindole (DAPI; blue). Scale bars, 10 μm. (**b**) Average fluorescence intensity of Numb in individual HSCs and progenitor cells. Data shown are from 2 independent experiments ($n = 34$ cells for each cell type). The difference between cell types was highly significant ($P < 0.0001$). Horizontal bars represent the mean values. (**c**) RT-PCR analysis of *Numb* expression in Lin$^-$ and Lin$^+$ cells ($n = 2$ independent experiments). (**d**) Representative images of individual HSC-enriched cells with polarized or non-polarized Numb (Numb is shown in red, DAPI is shown in blue; 63×). Scale bars, 2.5 μm. (**e**) Frequency of tamoxifen-treated control (*Lis1*$^{+/+}$; *Rosa26-creER*, indicated as WT) and tamoxifen-treated *Lis1*-floxed (*Lis1*$^{f/f}$; *Rosa26-creER*, indicated as *Lis1*$^{-/-}$) cells with polarized Numb. Frequencies were determined using 100 tracked cells for each genotype. (**f**) The model illustrates how two dividing cells may equivalently polarize Numb (red) to one side of the cell, yet direct the cleavage plane (dashed line) to ensure either equal or unequal inheritance of Numb by the incipient daughter cells. (**g**) Representative images of tracked cells showing inheritance of Numb symmetrically or asymmetrically by incipient daughter cells (Numb is shown in red, DAPI is shown in blue; 63×). Scale bars, 2.5 μm. (**h**) Relative ratios of symmetric to asymmetric division *in vitro*. Data shown are from 2 independent experiments; $n = 25$–27 dividing cells were assessed for each experiment per cohort. $^{**}P = 0.0032$. (**i**) Representative images of symmetric and asymmetric inheritance of Numb by incipient daughter cells *in vivo* (Numb in shown in red, DAPI is shown in blue; 63×). Scale bars, 2.5 μm. (**j**) Relative ratios of symmetric to asymmetric division *in vivo* (nine dividing cells were assessed for the control (*Lis1*$^{f/f}$ + vehicle; WT) group; eight dividing cells were assessed for the *Lis1*$^{-/-}$ (*Lis1*$^{f/f}$ + tam) group. Data were analyzed using three independent chimeric mice for each genotype. All error bars indicate the s.e.m.

HSCs also had normal frequencies of apoptotic cells (**Fig. 3d** and **Supplementary Fig. 9**). The fact that HSC depletion occurred as early as day 3 after *Lis1* deletion when no changes in cell survival were observed suggested that apoptosis is unlikely to account for HSC loss. Some increase in necrosis (**Supplementary Fig. 9**) could contribute to the overall phenotype; however, the fact that this necrosis occurred after HSC depletion was initiated suggested that loss of *Lis1* might influence stem cells through other mechanisms.

To test whether depletion of HSCs resulted from defects in the maintenance of the undifferentiated state, we tracked the rate of differentiation of *Lis1*-deficient cells. HSC-enriched cells from either *Lis1*$^{f/f}$; *creER* or control *Lis1*$^{+/+}$; *creER* mice were treated with tamoxifen at $t = 0$, and their differentiation was monitored (**Supplementary Fig. 10**). Over 24 h, ~23% of *Lis1*-null cells became positive for lineage markers (Lin$^+$), while only ~9% of control cells became positive for these markers (**Fig. 3e**,**f**). Notably, the increase in differentiation after *Lis1* deletion was not due to preferential death of immature (Lin$^-$) cells (**Fig. 3g**).

Because accelerated differentiation can be a consequence of defects in asymmetric cell division, we examined whether Lis1 loss led to altered polarization of fate determinants within mother cells or altered inheritance of these determinants by daughter cells. Numb is an important fate determinant that marks differentiated cells (**Fig. 4a**–**c**) and can accelerate differentiation upon ectopic expression[5]; conversely, Numb inhibition can also sustain cells in an undifferentiated state (**Supplementary Fig. 11**). We thus tracked the polarization and inheritance of Numb in HSC-enriched cells. Numb was distributed evenly in 63% of cells and was polarized in 37% of cells. Absence of *Lis1* did not affect Numb distribution (**Fig. 4d**,**e** and **Supplementary Fig. 12a**). In cells with polarized Numb, changes in the plane of division can lead to equal or unequal inheritance by the two daughter cells (**Fig. 4f**). To analyze changes in Numb inheritance, HSC-enriched cells from control mice or mice with the *loxP*-flanked *Lis1* allele were treated with tamoxifen *in vitro* (**Supplementary Fig. 12a**). Following *Lis1* deletion, cells were stained for Numb, and the ratio of symmetric to asymmetric division was determined. Only cells in late telophase or ones undergoing cytokinesis were tracked to assess Numb inheritance in incipient daughter cells. Cells either displayed equivalent distribution of low levels of Numb to both daughter cells (**Fig. 4g**, symmetric) or unequal distribution, i.e., with higher levels of Numb distributed to one daughter cell and lower levels distributed to the other (**Fig. 4g**, asymmetric). Control cells displayed twofold more symmetric inheritance relative to asymmetric inheritance of Numb. In contrast, *Lis1* loss led to a complete reversal in the pattern of inheritance, with twofold more cells undergoing asymmetric division (**Fig. 4h**).

We tested whether this shift in division pattern occurred after *Lis1* deletion *in vivo*. Because of the limited number of telophase HSCs *in vivo*, we focused on lineage-negative cells, a less enriched but nonetheless immature population. We analyzed Numb inheritance in incipient daughter cells from *Lis1*-null or control lineage-negative (Lin$^-$) cells (**Supplementary Fig. 12b**). Consistent with our *in vitro* analysis, control cells underwent symmetric divisions 3.5 times more frequently,

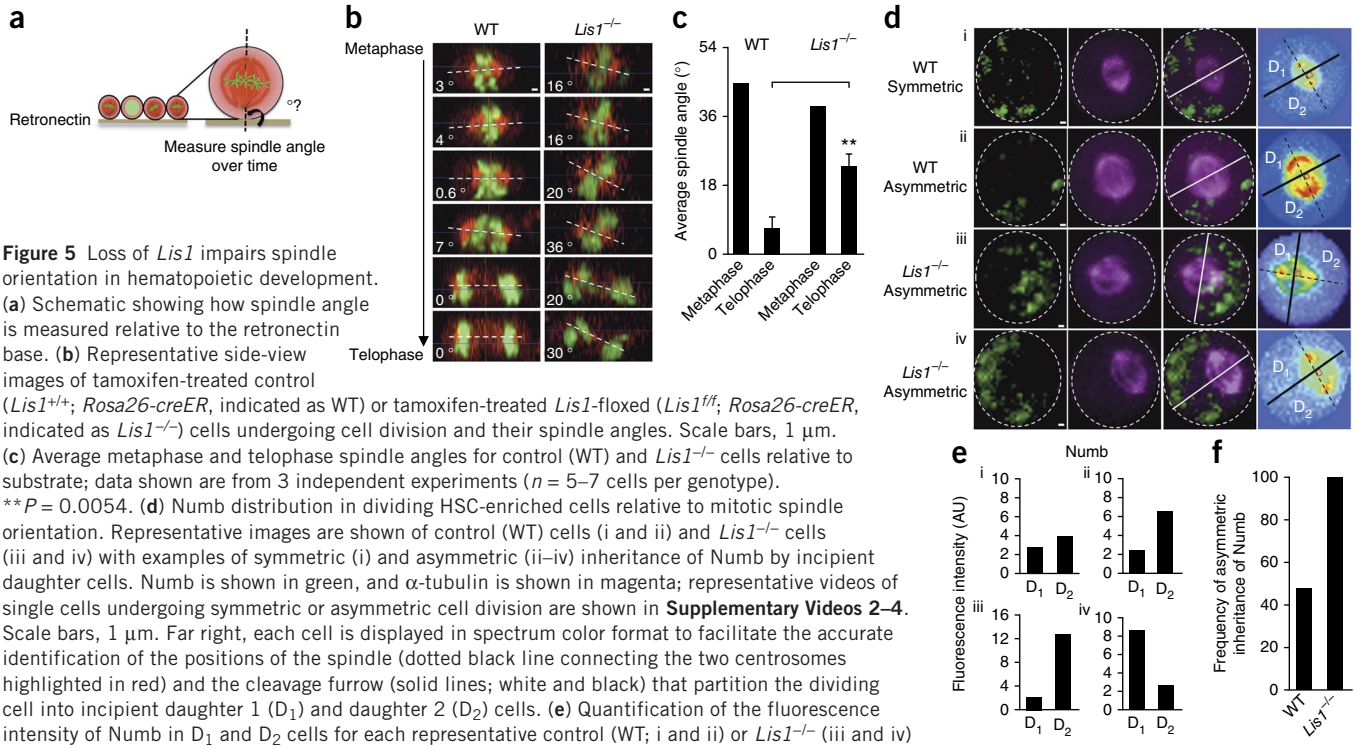

Figure 5 Loss of *Lis1* impairs spindle orientation in hematopoietic development. (**a**) Schematic showing how spindle angle is measured relative to the retronectin base. (**b**) Representative side-view images of tamoxifen-treated control (*Lis1*$^{+/+}$; *Rosa26-creER*, indicated as WT) or tamoxifen-treated *Lis1*-floxed (*Lis1*$^{f/f}$; *Rosa26-creER*, indicated as *Lis1*$^{-/-}$) cells undergoing cell division and their spindle angles. Scale bars, 1 μm. (**c**) Average metaphase and telophase spindle angles for control (WT) and *Lis1*$^{-/-}$ cells relative to substrate; data shown are from 3 independent experiments (n = 5–7 cells per genotype). $^{**}P = 0.0054$. (**d**) Numb distribution in dividing HSC-enriched cells relative to mitotic spindle orientation. Representative images are shown of control (WT) cells (i and ii) and *Lis1*$^{-/-}$ cells (iii and iv) with examples of symmetric (i) and asymmetric (ii–iv) inheritance of Numb by incipient daughter cells. Numb is shown in green, and α-tubulin is shown in magenta; representative videos of single cells undergoing symmetric or asymmetric cell division are shown in **Supplementary Videos 2–4**. Scale bars, 1 μm. Far right, each cell is displayed in spectrum color format to facilitate the accurate identification of the positions of the spindle (dotted black line connecting the two centrosomes highlighted in red) and the cleavage furrow (solid lines; white and black) that partition the dividing cell into incipient daughter 1 (D_1) and daughter 2 (D_2) cells. (**e**) Quantification of the fluorescence intensity of Numb in D_1 and D_2 cells for each representative control (WT; i and ii) or *Lis1*$^{-/-}$ (iii and iv) cell shown in **d**. AU, arbitrary units. (**f**) Frequency of cells undergoing asymmetric inheritance of Numb in control (WT) and *Lis1*$^{-/-}$ cells; data are shown for 4 independent experiments (n = 23 WT cells and 9 *Lis1*$^{-/-}$ cells). All error bars, s.e.m.

and loss of *Lis1* led to a predominance of asymmetric divisions. This shift led to a sevenfold difference in the ratio of symmetric to asymmetric divisions between control and *Lis1*-deficient cells (**Fig. 4i,j**). Because *Lis1* deletion affected Numb inheritance but not Numb polarization, these data cumulatively suggest that the absence of Lis1 affects inheritance by changing the cleavage plane (**Fig. 4f**), thereby generating more cells that have higher levels of Numb.

Lis1 controls spindle orientation in hematopoietic stem cells

To directly test whether loss of Lis1 leads to changes in the cleavage plane and whether this results from defects in spindle positioning, we developed a strategy to image spindle orientation during cell division in real time. This imaging approach was a modification of a method previously used to visualize spindles in epithelial lines[19]. Cells were infected with viral constructs for H2B-GFP[20] to mark separating chromosomes and mCherry–α-tubulin[21] to mark spindles (**Supplementary Fig. 13** and **Supplementary Video 1**). Cells were plated on retronectin and imaged; four-dimensional (x, y, z, t) movies of dividing cells were visualized from the side to measure the spindle angle relative to the substrate. Whereas a range of spindle angles was seen in metaphase, the spindle was always positioned parallel (0–10 °) to the substrate in telophase, consistent with previous reports[19]. This substrate-directed repositioning of the mitotic spindle allowed us to test whether Lis1 controls spindle orientation in hematopoietic cells. Control HSC-enriched cells displayed a range of angles during metaphase but repositioned their spindles by telophase (**Fig. 5a–c**). In contrast, *Lis1*-deficient cells were unable to correctly position their spindles (**Fig. 5a–c**). These data suggest that Lis1 loss leads to defects in spindle orientation in HSC-enriched cells.

Finally, we tested whether the spindle orientation defects driven by *Lis1* deficiency led to the improper inheritance of Numb. Thus, we tracked the orientation of the spindle coordinately with Numb inheritance in real time. HSC-enriched cells were infected with mCherry–α-tubulin and Numb-CFP; subsequently, Numb inheritance was tracked relative to the mitotic spindle using time-lapse microscopy (**Supplementary Videos 2–4**). Of the cells entering mitosis, we focused on those with polarized Numb because changes in the spindle angle would determine whether Numb was inherited asymmetrically or symmetrically only in these cells (non-polarized cells should invariably undergo symmetric division regardless of spindle orientation). Live imaging of control and *Lis1*-null primary stem and progenitor cells yielded clear and distinct patterns. Whereas the mitotic spindle was positioned such that Numb was bisected asymmetrically in 56.5% of wild-type cells, the mitotic spindle bisected Numb asymmetrically in 100% of the *Lis1*-null cells (**Fig. 5d–f**). The functional consequence of spindle positioning in stem cells was tested by ectopic expression of Nde1, a protein that independently controls spindle orientation[22]. Expression of this protein conferred a partial rescue of the accelerated differentiation seen in *Lis1*-deficient stem cells (**Supplementary Fig. 14**). These data suggest that defective spindle positioning in the absence of Lis1 increases asymmetric inheritance of Numb and accelerates differentiation, identifying these changes as a mechanism that underlies, at least in part, the HSC depletion observed in *Lis1*-null cells.

Although the absence of Lis1 affects spindle orientation, it may also affect other aspects of stem cell function. Because Lis1 is linked to spindle assembly, we tested whether *Lis1* deficiency affected bipolar spindle formation, spindle morphology or nuclear envelope breakdown and were unable to identify any obvious defects (**Supplementary Fig. 15**). In addition, no significant changes in mitotic duration were observed in the absence of *Lis1* (**Supplementary Fig. 15**). However, an increase in the number of cells with abnormal mitoses (multipolar or incomplete) did occur (**Supplementary Fig. 15**). It is thus possible that, in addition to defects in spindle orientation and the inheritance of fate determinants, some loss of cells with abnormal mitoses (possibly linked to

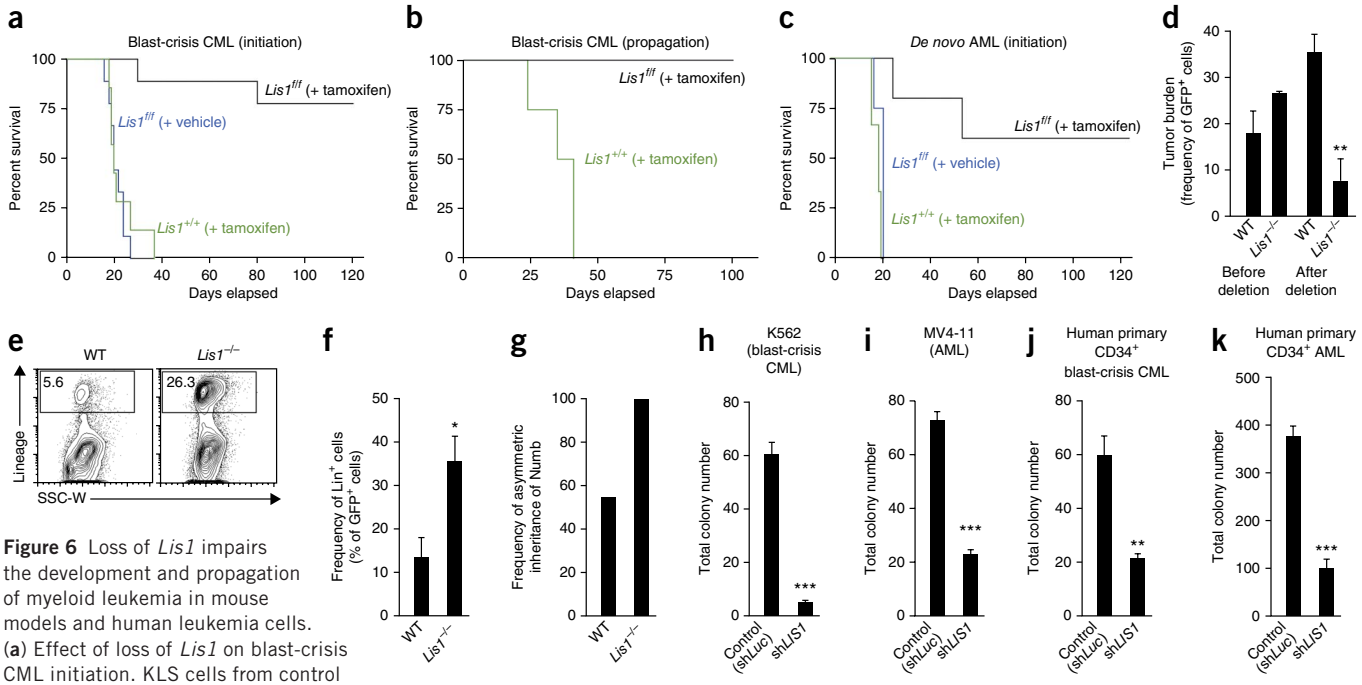

Figure 6 Loss of *Lis1* impairs the development and propagation of myeloid leukemia in mouse models and human leukemia cells. (**a**) Effect of loss of *Lis1* on blast-crisis CML initiation. KLS cells from control (*Lis1*$^{+/+}$; *Rosa26-creER*, *Lis1*$^{+/+}$) and *Lis1*$^{f/f}$; *Rosa26-creER* (*Lis1*$^{f/f}$) mice transduced with viral constructs for BCR-ABL-IRES-YFP and NUP98-HOXA9-IRES-GFP were transplanted into recipients and treated with tamoxifen, and survival was monitored. Data shown are from 3 independent experiments ($n = 9$ for *Lis1*$^{f/f}$ + tamoxifen, 9 for *Lis1*$^{f/f}$ + vehicle and 7 for *Lis1*$^{+/+}$ + tamoxifen). (**b**) Effect of loss of *Lis1* on the propagation of established blast-crisis CML. Lin$^-$ cells from established control *Lis1*$^{+/+}$; *creER* or *Lis1*$^{f/f}$; *creER* blast-crisis CML were transplanted into secondary recipients. Recipients were administered tamoxifen, and survival was monitored ($n = 4$ for *Lis1*$^{+/+}$ and 3 for *Lis1*$^{f/f}$). (**c**) Effect of loss of *Lis1* on *de novo* AML. KLS cells were isolated from control (*Lis1*$^{+/+}$; *Rosa26-creER*) and *Lis1*$^{f/f}$; *Rosa26-creER* mice, cotransduced with constructs for MLL-AF9-IRES-GFP and NRAS^{G12V}-IRES-YFP and treated with tamoxifen or corn oil, and survival was monitored. Data shown are from 2 experiments ($n = 5$ for *Lis1*$^{f/f}$ + tamoxifen, 4 for *Lis1*$^{f/f}$ + vehicle and 3 for *Lis1*$^{+/+}$ + tamoxifen). (**d**–**f**) Growth and cellular behavior of blast-crisis CML *in vivo*. (**d**) Lin$^-$ cells from control *Lis1*$^{+/+}$; *Rosa26-creER* or *Lis1*$^{f/f}$; *Rosa26-creER* established blast-crisis CML were transplanted into secondary recipients, and average tumor burden was tracked before (percentage of peripheral blood) and after (percentage of spleen cells) tamoxifen delivery; $n = 4$ for control (WT) and 3 for *Lis1*$^{-/-}$ mice. $^{**}P = 0.0065$. (**e**) Representative FACS plots show the frequency of blast-crisis CML cells expressing lineage markers (boxed) in control (WT) or *Lis1*$^{-/-}$ populations 1 d after tamoxifen treatment. SSC-W, side scatter width. (**f**) Average frequency of blast-crisis CML cells expressing lineage markers (Lin$^+$). Data shown are from 2 independent experiments ($n = 4$ for WT and 6 for *Lis1*$^{-/-}$). $^{*}P = 0.0282$. (**g**) Frequency of leukemia cells undergoing asymmetric inheritance of Numb in control (WT) or *Lis1*$^{-/-}$ cells; $n = 22$ cells for WT and 7 for *Lis1*$^{-/-}$. (**h**–**k**) Influence of *Lis1* loss on human leukemia growth. Human leukemia cells were infected with lentiviral constructs expressing either control shRNA (sh*Luc*) or shRNA targeting human *LIS1* (sh*LIS1*). Subsequently, infected cells were sorted and plated in methylcellulose. Colony formation was assessed in K562 blast-crisis CML cells (**h**), MV4-11 AML cells (**i**), primary human CD34$^+$ blast-crisis CML samples resistant to imatinib, nilotinib and dasatinib (**j**) and primary human CD34$^+$ AML (**k**). One patient sample was tested for each leukemia with $n = 3$ technical replicates. $^{**}P < 0.01$, $^{***}P < 0.001$. All error bars, s.e.m.

late-onset necrosis as seen in **Supplementary Fig. 9d**) contributes to the overall defects observed in the absence of *Lis1*.

Lis1 is required for mouse and human myeloid leukemias

Whereas proper regulation of the stem cell state is a critical feature of normal development, aberrant adoption of stem cell programs can be a hallmark of oncogenesis[23]. Whether regulators of spindle orientation and division plane can contribute to cancer is an important question that remains unaddressed. This may be particularly relevant in understanding the regulation of immature cancers and cancer stem cells, as a shift toward symmetric renewal divisions could contribute to the failure of differentiation and maintenance of a stem cell state. In the hematopoietic system, acute-phase myeloid leukemias such as blast-crisis CML and *de novo* AML display a severe differentiation blockade. We thus used these leukemias as models to test whether Lis1 has a role in blood cancers.

To generate blast-crisis CML, HSCs from *Lis1*$^{+/+}$; *creER* and *Lis1*$^{f/f}$; *creER* mice were coinfected with viral constructs for BCR-ABL and NUP98-HOXA9 (refs. 24–26) and transplanted into sublethally irradiated mice. Mice were then treated with tamoxifen or corn oil. Whereas all tamoxifen-treated mice transplanted with control cells expressing BCR-ABL and NUP98-HOXA9 succumbed to blast-crisis CML, only 22% of the tamoxifen-treated mice transplanted with *Lis1*$^{f/f}$; *creER* cells expressing BCR-ABL or NUP98-HOXA9 developed leukemia (**Fig. 6a**). The ability to temporally control *Lis1* loss also allowed us to delete *Lis1* after disease establishment. Established blast-crisis CML cells with a *loxP*-flanked *Lis1* allele were transplanted into recipient mice that were subsequently treated with tamoxifen. Whereas all mice transplanted with control leukemia-propagating cells succumbed to leukemia, none of the mice transplanted with cells that conditionally lost *Lis1* developed leukemia (**Fig. 6b**). This finding indicated that Lis1 is critically important for both the establishment and continued propagation of blast-crisis CML. Notably, a similar impairment in leukemia growth occurred in *de novo* AML induced by coexpression of the human mixed-lineage leukemia fusion protein (MLL-AF9) and NRAS^{G12V} (ref. 27). Whereas all control mice died of leukemia within 3 weeks, only ~40% of mice transplanted with cells that conditionally lost *Lis1* developed AML, and those that died exhibited longer disease latency (**Fig. 6c**).

To understand the cellular and molecular impact of *Lis1* deletion on leukemogenesis, we used the blast-crisis CML model. Monitoring GFP-positive leukemia cells, we found that deletion of *Lis1* well after

the tumor burden had begun to increase allowed complete reversion to normal cell counts and resolution of disease (**Fig. 6d** and **Supplementary Fig. 16a**,**b**). At a cellular level, the most notable and immediate impact of *Lis1* deletion was a fivefold increase in the number of differentiated leukemic cells (**Fig. 6e**,**f**), accompanied by an increase in Numb expression (**Supplementary Fig. 16c**,**d**). In addition, real-time imaging showed that, whereas Numb was bisected asymmetrically in 54.5% of control leukemia cells, it was bisected asymmetrically in 100% of *Lis1*-null cells (**Fig. 6g** and **Supplementary Fig. 17**). This observation suggests that incorrectly directed Numb inheritance could be a possible basis for the increased Numb expression and differentiation observed in *Lis1*-deficient leukemia cells. In addition, *Lis1* loss led to a 1.5-fold reduction in proliferation; thus, the differentiation and proliferation defects may act together to lead to the severe defects observed in leukemogenesis. Consistent with our observations in normal HSCs, loss of *Lis1* in leukemic cells did not cause any defects in apoptosis (data not shown).

To test whether Lis1 is also required for human myeloid leukemia, we deleted *LIS1* (also known as *PAFAH1B1*) in leukemic cell lines and primary human samples. The blast-crisis CML cell line K562 and the *de novo* AML cell line MV4-11 were infected with viruses expressing short hairpin RNA (shRNA) targeting *LIS1*; colony-forming ability was then measured. Knockdown of *LIS1* led to a significant reduction in the colony-forming ability of both leukemia cell lines (**Fig. 6h**,**i** and **Supplementary Fig. 18**). We tested the role of LIS1 in primary human leukemia by infecting patient-derived $CD34^+$ blast-crisis CML cells resistant to the tyrosine kinase inhibitors imatinib, nilotinib and dasatinib as well as $CD34^+$ AML patient-derived cells harboring the therapy-resistant *MLL-AF9* (*KMT2A-MLLT3*) translocation with shRNA to *LIS1* and assessed colony formation. As shown (**Fig. 6j**,**k** and **Supplementary Fig. 18**), inhibition of *LIS1* expression led to marked blockade of colony-forming ability in both cancers. To understand the basis of the decrease in colony formation, we analyzed the consequence of *LIS1* knockdown on growth and differentiation. Inhibition of *LIS1* in primary, patient-derived AML samples did not affect cell growth in the short term (24–72 h) but led to accelerated differentiation, as indicated by the increased frequency of MAC-1–expressing cells (**Supplementary Fig. 19**). Because the viability of primary, patient-derived myeloid leukemia samples decreases substantially after short-term culture, longer term analysis of proliferation was carried out in cell lines; inhibition of *LIS1* led to a decease in cell numbers over a period of 12 d (data not shown). These data collectively suggest that inhibition of *LIS1* increases differentiation in the short term and blocks growth in the longer term (either as a consequence of or independent of differentiation) and identify LIS1 as a critical new regulator of human leukemia growth and propagation.

DISCUSSION

The studies described here show that Lis1 is critically required for the development of the hematopoietic system. Its loss in mice leads to a bloodless embryo and severe defects in HSC maintenance and expansion in both fetal and adult life. Such an effect on fetal hematopoiesis has previously been reported largely for key transcription factors such as Runx1 (Aml1), Scl (Tal-1) and Gata2 (refs. 28–31). In this context, the influence of Lis1 on the hematopoietic system implicates proteins that direct asymmetric division as a new class of regulators of hematopoiesis.

Our data indicate that a predominant genomic consequence of *Lis1* deletion is loss of the stem cell core gene signature, suggesting that Lis1 is critical for the maintenance of the stem cell state. How *Lis1* deletion leads to loss of the stem cell state could potentially involve defects in the inheritance of cell fate determinants. As depicted in our model (**Supplementary Fig. 20**), if loss of Lis1 leads to incorrect spindle positioning and thus triggers an increase in asymmetric division, more cells would inherit high levels of Numb. This would in turn generate a greater number of differentiated cells with each division. Thus, if more differentiated cells comprise a greater fraction and the undifferentiated stem cells comprise a smaller fraction of the KLS population used in the array analysis, this might lead to reduction in or loss of the stem cell signature observed. It is also possible that Lis1 affects the stem cell core signature through as yet unknown mechanisms that are unrelated to its role in spindle positioning and asymmetric division.

Our results show that the stem cell defects that occur in the absence of Lis1 are linked to increased inheritance of Numb and a marked imbalance in asymmetric and symmetric divisions. These findings identify Lis1 as a key component of the molecular machinery that directs asymmetric division in HSCs and provide, to our knowledge, the first genetic proof for the requirement of a proper balance of asymmetric division and its regulators for hematopoietic development *in vivo*. Defining the position and orientation of the immature hematopoietic cells within their microenvironment would be an important aspect of future work, as environmental cues may be critical for specifying the plane of division of hematopoietic cells through Lis1. Although our focus has been on understanding the severe reduction in the stem cell pool, we found possibly independent defects in mature erythroid and granulocyte lineages. Interestingly, these findings parallel those of mice lacking the serine-threonine kinase Lkb1 (refs. 32,33), which exhibit defects in HSCs. The role of Lkb1 in asymmetric division[34] raises the possibility that Lkb1 and Lis1 control overlapping, albeit not identical, mechanisms in the hematopoietic system.

Elucidating the basis of the maintenance of the undifferentiated state is important because it may allow an understanding of the mechanisms underlying the differentiation blockade seen in cancers such as glioblastoma, breast cancer and leukemia[35–37]. Emerging studies indicate that the presence and dysregulated expression of fate determinants such as Numb and Musashi may be important elements of the induction of such cancers[10,38]. Our work now shows that the regulatory mechanisms that direct the inheritance of these determinants are perhaps equally important for the establishment and continued propagation of malignancies. Previous studies have shown that loss of proteins involved in asymmetric division, including Brat, Prospero and Numb, can trigger tumor formation in *Drosophila* neuroblasts[39–44]. These findings identify Lis1 as a key component of the molecular machinery that directs asymmetric division in HSCs. To our knowledge, this work provides the first genetic evidence that asymmetric division and the mechanisms that direct it are required for hematopoietic development. This connection raises the possibility that the molecules that can control or modulate the inheritance of fate determinants could serve as a powerful new class of regulators of cancer growth and that further work in this area may define new approaches to therapy.

METHODS

Methods and any associated references are available in the online version of the paper.

Accession codes. Microarray data reported here have been deposited in the ArrayExpress database (accession E-MEXP-3855).

Note: Any Supplementary Information and Source Data files are available in the online version of the paper.

ACKNOWLEDGMENTS

We are grateful to B. Hogan, J. Chang, A. Desai, J. Gleeson, J.E. Lee, M.F. Wu, M. Sander and J. Koop for experimental advice and reagents. We would also like to thank M. Kritzik for advice and comments on the manuscript; M. Nakamura for experimental help; M. Cook, L. Matinek, B. Harvat, E. O'Conner and K. Marquez for cell sorting; and W. Pear (University of Pennsylvania) and A.M. Pendergast (Duke University) for the BCR-ABL construct, D.G. Gilliland (University of Pennsylvania) for the NUP98-HOXA9 construct, S. Armstrong (Memorial Sloan-Kettering Cancer Center) for the MLL-AF9 construct, C. Counter (Duke University) for $NRAS^{G12V}$, S. Russell (Peter MacCallum Cancer Centre) for the mCherry–α-tubulin construct, G. Wahl (Salk Institute) for the H2B-GFP (pEGFPN1) vector and D. Kioussis (Medical Research Council National Institute for Medical Research) for the *Vav1-cre* transgenic line. B.Z. and C.S.K. received support from US National Institutes of Health (NIH) Cancer Biology Training Grant (T32 CA 59365-18) and NIH Pharmacological Sciences Training Program (T32 GM007752), respectively. T.I. is a recipient of a California Institute for Regenerative Medicine interdisciplinary stem cell training program fellowship, and T.K. is supported by a postdoctoral fellowship from the Japanese Society for the Promotion of Science. This work was also supported by a Leukemia and Lymphoma Society Scholar Award, the University of California San Diego Moores Cancer Center National Cancer Institute Core Grant, P30CA23100, as well as by NIH grants DK63031, HL097767 and DP1 CA174422 awarded to T.R.

AUTHOR CONTRIBUTIONS

B.Z. and T.I. planned and designed the research, performed the majority of experiments and helped write the manuscript. B.Z. and J.B. developed all real-time imaging methods for visualizing and tracking spindle orientation in primary hematopoietic cells. A.B., J.B., T.K., J.W., C.S.K., H.Y.K. and O.A. provided experimental data and help. D.R., H.E.B., C.C. and V.G.O. provided primary patient samples and experimental advice. R.S. and G.H. carried out all bioinformatics analysis on microarray data. T.R. planned and guided the project, provided experimental advice and wrote the manuscript.

COMPETING FINANCIAL INTERESTS

The authors declare no competing financial interests.

1. Siller, K.H. & Doe, C.Q. Lis1/dynactin regulates metaphase spindle orientation in *Drosophila* neuroblasts. *Dev. Biol.* **319**, 1–9 (2008).
2. Yingling, J. *et al.* Neuroepithelial stem cell proliferation requires LIS1 for precise spindle orientation and symmetric division. *Cell* **132**, 474–486 (2008).
3. Suda, T., Suda, J. & Ogawa, M. Disparate differentiation in mouse hemopoietic colonies derived from paired progenitors. *Proc. Natl. Acad. Sci. USA* **81**, 2520–2524 (1984).
4. Ting, S.B. *et al.* Asymmetric segregation and self-renewal of hematopoietic stem and progenitor cells with endocytic Ap2a2. *Blood* **119**, 2510–2522 (2012).
5. Wu, M. *et al.* Imaging hematopoietic precursor division in real time. *Cell Stem Cell* **1**, 541–554 (2007).
6. Hope, K.J. *et al.* An RNAi screen identifies *Msi2* and *Prox1* as having opposite roles in the regulation of hematopoietic stem cell activity. *Cell Stem Cell* **7**, 101–113 (2010).
7. Ito, K. *et al.* Regulation of reactive oxygen species by Atm is essential for proper response to DNA double-strand breaks in lymphocytes. *J. Immunol.* **178**, 103–110 (2007).
8. Kharas, M.G. *et al.* Musashi-2 regulates normal hematopoiesis and promotes aggressive myeloid leukemia. *Nat. Med.* **16**, 903–908 (2010).
9. de Andrés-Aguayo, L. *et al.* Musashi 2 is a regulator of the HSC compartment identified by a retroviral insertion screen and knockout mice. *Blood* **118**, 554–564 (2011).
10. Ito, T. *et al.* Regulation of myeloid leukaemia by the cell-fate determinant Musashi. *Nature* **466**, 765–768 (2010).
11. Hirotsune, S. *et al.* Graded reduction of *Pafah1b1* (*Lis1*) activity results in neuronal migration defects and early embryonic lethality. *Nat. Genet.* **19**, 333–339 (1998).
12. de Boer, J. *et al.* Transgenic mice with hematopoietic and lymphoid specific expression of Cre. *Eur. J. Immunol.* **33**, 314–325 (2003).
13. Almarza, E. *et al.* Regulatory elements of the *vav* gene drive transgene expression in hematopoietic stem cells from adult mice. *Exp. Hematol.* **32**, 360–364 (2004).
14. Ogilvy, S. *et al.* Promoter elements of *vav* drive transgene expression *in vivo* throughout the hematopoietic compartment. *Blood* **94**, 1855–1863 (1999).
15. Ventura, A. *et al.* Restoration of p53 function leads to tumour regression *in vivo*. *Nature* **445**, 661–665 (2007).
16. Wong, D.J. *et al.* Module map of stem cell genes guides creation of epithelial cancer stem cells. *Cell Stem Cell* **2**, 333–344 (2008).
17. Venezia, T.A. *et al.* Molecular signatures of proliferation and quiescence in hematopoietic stem cells. *PLoS Biol.* **2**, e301 (2004).
18. Eppert, K. *et al.* Stem cell gene expression programs influence clinical outcome in human leukemia. *Nat. Med.* **17**, 1086–1093 (2011).
19. Toyoshima, F. & Nishida, E. Integrin-mediated adhesion orients the spindle parallel to the substratum in an EB1- and myosin X–dependent manner. *EMBO J.* **26**, 1487–1498 (2007).
20. Kanda, T., Sullivan, K.F. & Wahl, G.M. Histone-GFP fusion protein enables sensitive analysis of chromosome dynamics in living mammalian cells. *Curr. Biol.* **8**, 377–385 (1998).
21. Day, D. *et al.* A method for prolonged imaging of motile lymphocytes. *Immunol. Cell Biol.* **87**, 154–158 (2009).
22. Feng, Y. & Walsh, C.A. Mitotic spindle regulation by Nde1 controls cerebral cortical size. *Neuron* **44**, 279–293 (2004).
23. Reya, T., Morrison, S.J., Clarke, M.F. & Weissman, I.L. Stem cells, cancer, and cancer stem cells. *Nature* **414**, 105–111 (2001).
24. Dash, A.B. *et al.* A murine model of CML blast crisis induced by cooperation between BCR/ABL and NUP98/HOXA9. *Proc. Natl. Acad. Sci. USA* **99**, 7622–7627 (2002).
25. Mayotte, N., Roy, D.C., Yao, J., Kroon, E. & Sauvageau, G. Oncogenic interaction between *BCR-ABL* and *NUP98-HOXA9* demonstrated by the use of an *in vitro* purging culture system. *Blood* **100**, 4177–4184 (2002).
26. Neering, S.J. *et al.* Leukemia stem cells in a genetically defined murine model of blast-crisis CML. *Blood* **110**, 2578–2585 (2007).
27. Zuber, J. *et al.* Mouse models of human AML accurately predict chemotherapy response. *Genes Dev.* **23**, 877–889 (2009).
28. Tsai, F.Y. *et al.* An early haematopoietic defect in mice lacking the transcription factor GATA-2. *Nature* **371**, 221–226 (1994).
29. Wang, Q. *et al.* Disruption of the *Cbfa2* gene causes necrosis and hemorrhaging in the central nervous system and blocks definitive hematopoiesis. *Proc. Natl. Acad. Sci. USA* **93**, 3444–3449 (1996).
30. Okuda, T., van Deursen, J., Hiebert, S.W., Grosveld, G. & Downing, J.R. *AML1*, the target of multiple chromosomal translocations in human leukemia, is essential for normal fetal liver hematopoiesis. *Cell* **84**, 321–330 (1996).
31. Porcher, C. *et al.* The T cell leukemia oncoprotein SCL/tal-1 is essential for development of all hematopoietic lineages. *Cell* **86**, 47–57 (1996).
32. Gan, B. *et al.* Lkb1 regulates quiescence and metabolic homeostasis of haematopoietic stem cells. *Nature* **468**, 701–704 (2010).
33. Nakada, D., Saunders, T.L. & Morrison, S.J. Lkb1 regulates cell cycle and energy metabolism in haematopoietic stem cells. *Nature* **468**, 653–658 (2010).
34. Bonaccorsi, S. *et al.* The *Drosophila* Lkb1 kinase is required for spindle formation and asymmetric neuroblast division. *Development* **134**, 2183–2193 (2007).
35. Calabretta, B. & Perrotti, D. The biology of CML blast crisis. *Blood* **103**, 4010–4022 (2004).
36. Stingl, J. & Caldas, C. Molecular heterogeneity of breast carcinomas and the cancer stem cell hypothesis. *Nat. Rev. Cancer* **7**, 791–799 (2007).
37. Maher, E.A. *et al.* Malignant glioma: genetics and biology of a grave matter. *Genes Dev.* **15**, 1311–1333 (2001).
38. Pece, S. *et al.* Loss of negative regulation by Numb over Notch is relevant to human breast carcinogenesis. *J. Cell Biol.* **167**, 215–221 (2004).
39. Bello, B., Reichert, H. & Hirth, F. The brain tumor gene negatively regulates neural progenitor cell proliferation in the larval central brain of *Drosophila*. *Development* **133**, 2639–2648 (2006).
40. Betschinger, J., Mechtler, K. & Knoblich, J.A. Asymmetric segregation of the tumor suppressor Brat regulates self-renewal in *Drosophila* neural stem cells. *Cell* **124**, 1241–1253 (2006).
41. Caussinus, E. & Gonzalez, C. Induction of tumor growth by altered stem-cell asymmetric division in *Drosophila melanogaster*. *Nat. Genet.* **37**, 1125–1129 (2005).
42. Lee, C.Y. *et al.* *Drosophila* Aurora-A kinase inhibits neuroblast self-renewal by regulating aPKC/Numb cortical polarity and spindle orientation. *Genes Dev.* **20**, 3464–3474 (2006).
43. Lee, C.Y., Wilkinson, B.D., Siegrist, S.E., Wharton, R.P. & Doe, C.Q. Brat is a Miranda cargo protein that promotes neuronal differentiation and inhibits neuroblast self-renewal. *Dev. Cell* **10**, 441–449 (2006).
44. Wang, H. *et al.* Aurora-A acts as a tumor suppressor and regulates self-renewal of *Drosophila* neuroblasts. *Genes Dev.* **20**, 3453–3463 (2006).

ONLINE METHODS

Generation and analysis of mice. Hypomorphic conditional knockout mice (*Lis1*$^{f/f}$; strain: 129-*Pafah1b1*$^{tm2awb/J}$)[11] were mated with either *Rosa26-creER* mice (strain: B6;*129-Gt(ROSA)26Sor*$^{tm1(cre/Esr1)Tyj}$)[15] or *Vav1-cre* transgenic mice[12]. Vav1-Cre reporter mice were generated by crossing *Vav1-cre* mice to *Rosa26-stop-tdTomato* mice (strain: B6.Cg-*Gt(ROSA)26Sor*$^{tm9(CAG-tdTomato)Hze}$/J; stock 007909). B6-CD45.1 (strain B6.SJL-*Ptprc*^{a}*Pepc*^{b}/BoyJ) mice were used as transplant recipients. All mice were 6–16 weeks of age and were gender and age matched for experiments. Mice were bred and maintained in the animal care facilities at Duke University Medical Center and the University of California, San Diego. Tamoxifen treatment was carried out as previously described[45]. In brief, adult mice were administered tamoxifen (Sigma) in corn oil (20 mg/ml) daily by oral gavage at ~114 µg of tamoxifen per gram of body weight per day for 5 consecutive days. For leukemia experiments, all recipient mice weighed ~17.5–20 g and were administered 2 mg of tamoxifen per day for 5 consecutive days. Embryos were suspended in PBS and visualized with a Leica MZ16 FA Fluorescence Stereomicroscope. Embryos were fixed in 4% paraformaldehyde and embedded in paraffin according to standard protocols. Sections (5 µm) were obtained for staining with hematoxylin and eosin. All animal experiments were performed according to protocols approved by the Duke University and University of California, San Diego Institutional Animal Care and Use Committees.

Cell isolation and FACS analysis. Cells were suspended in Hanks' balanced salt solution (HBSS) (Gibco, Life Technologies) containing 5% FBS and 2 mM EDTA and were prepared for FACS analysis and sorting as previously described[46]. The following antibodies were used to define lineage positive cells: 145-2C11 (CD3ε), GK1.5 (CD4), 53-6.7 (CD8), RB6-8C5 (Ly-6G/Gr1), M1/70 (CD11b/Mac-1), TER119 (Ly-76/TER119), 6B2 (CD45R/B220) and MB19-1 (CD19). Red blood cells were lysed using RBC Lysis Buffer (eBioscience) before staining for lineage markers. For fetal liver cell isolation and FACS analysis, single-cell suspensions were prepared by disaggregation and passage through a 74-µm nylon mesh (Corning). For fetal HSC population analysis, the lineage antibody cocktail was used without antibody to Mac-1. The following additional antibodies were used to define HSC populations: 2B8 (CD117/c-kit), D7 (Ly-6A/E/Sca-1), AA4.1 (CD93/C1qRp), HM48-1 (CD48/BCM1), TC15-12F12.2 (CD150) and A2F10 (CD135/Flt3). Fetal HSCs were defined as c-Kit^{+}Lin^{-}AA4.1^{+} (KL AA4.1^{+}). Adult HSCs were defined as either c-Kit^{+}Lin^{-}Sca1^{+}CD48^{-}CD150^{+} (KLS CD48^{-}CD150^{+}) or c-Kit^{+}Lin^{-}Sca1^{+}Flt3^{-} (KLSF). To determine donor-derived chimerism in transplantation-based assays, peripheral blood from recipients was obtained by the submandibular bleeding method and prepared for analysis as previously described[10]. All antibodies were purchased from eBioscience except TC15-12F12.2 (CD150), which was purchased from BioLegend. All antibodies were used at 0.5–1 µg/1 x 10^{6} cells. Apoptosis assays were performed by staining cells with Annexin V and 7-AAD (BD Pharmingen). Analysis of *in vivo* BrdU incorporation was performed using the FITC BrdU Flow kit (BD Pharmingen) after a single intraperitoneal injection of BrdU (2 mg). Analysis and cell sorting were carried out on FACSVantage SE, FACStar, FACSCanto II, FACSDiva and FACSAria III machines (all from Becton Dickinson), and data were analyzed with FlowJo software (Tree Star).

Retroviral and lentiviral constructs and production. MIG-BCR-ABL was a gift from W. Pear and A.M. Pendergast and was cloned into the MSCV-IRES-YFP retroviral vector. MSCV-NUP98-HOXA9-IRES-YFP was a gift from G. Gilliland and was cloned into the MSCV-IRES-GFP vector. MSCV-MLL-AF9-IRES-GFP was generously provided by S. Armstrong. cDNA encoding NRAS^{G12V} was a gift from C. Counter and was cloned into the MSCV-IRES-YFP retroviral vector. *Numb* cDNA (encoding the p65 isoform; NCBI accession BC033459) was either cloned into the MSCV-IRES-GFP vector or fused to CFP by cloning downstream of the IRES in the MSCV-IRES-CFP backbone. The shRNA construct targeting *Numb* was designed and cloned into the MSCV/LTRmiR30-PIG (LMP) vector from Open Biosystems according to the manufacturer's instructions. Mouse *Nde1* cDNA (NCBI accession BC023267) was cloned into the MSCV-IRES-GFP. H2B-GFP (pEGFPN1) vector[20] was a gift from G. Wahl, and the H2B-GFP chimeric gene was cloned into the MSCV-IRES-GFP retroviral vector following the removal of IRES-GFP. mCherry–α-tubulin fusion construct[21] was generously provided by J. Chang and S. Russell. Lentiviral shRNA constructs were cloned into FG12 as described previously[47]. Virus was produced in 293T (ATCC) cells transfected using FuGENE 6 or X-tremeGENE HP (Roche) with viral constructs along with VSV-G and gag-pol. For lentivirus production, Rev was also cotransfected. Viral supernatants were collected for 3 to 5 d and were ultracentrifuged at 50,000*g* for 3 h.

Cell culture and methylcellulose colony formation. For liquid culture, freshly isolated adult KLS (c-Kit^{+}Lin^{-}Sca-1^{+}) cells were plated into a 96-well U-bottom plate in X-Vivo15 (with gentamicin and phenol red) (Lonza) supplemented with 50 µM 2-mercaptoethanol, 10% FBS, stem cell factor (SCF; 100 ng/ml; R&D Systems) and thrombopoietin (TPO; 20 ng/ml; R&D Systems). 4-OH tamoxifen (Sigma) was dissolved in ethanol at 1 mg/ml (1,000×), and a 1× solution was made immediately before treatment. For certain immunofluorescence experiments, cells were treated for 24 h with either 10 µM cytochalasin B (Sigma) or 10 nM nocodazole (Sigma). For fetal liver methylcellulose assays, individual fetal livers from E12.5 embryos were dissected in cold PBS, disaggregated and passed through a 74-µm nylon mesh (Corning) to generate single-cell suspensions. Fetal liver cells (5,000) were plated in triplicate in Iscove's modified medium–based methylcellulose medium (Methocult M3434, StemCell Technologies). Erythroid (BFU-E) hematopoietic progenitors were scored by morphological criteria on day 7, and myeloid (CFU-GM) and multilineage (CFU-GEMM) colonies were scored on day 10.

***In vivo* transplantation assays.** For fetal liver transplants, 5,000 Lin^{-}AA4.1^{+} fetal liver cells (derived from E14.5 embryos expressing CD45.2) along with 3 × 10^{5} competitive bone marrow cells derived from an unirradiated recipient mouse were transplanted by retro-orbital intravenous injection into lethally irradiated (9.5 Gy) congenic recipient mice (expressing CD45.1). Recipient mice received donor cells derived from one individual embryo of a given genotype. Peripheral blood of recipient mice was collected at 4, 8, 12 and 16 weeks after transplantation. Donor and recipient cells were distinguished by expression of CD45.1 (A20; eBioscience) and CD45.2 (104; eBioscience). These antibodies were used at 0.5–1 µg/1 × 10^{6} cells. For bone marrow transplants, 500 LT-HSCs (c-Kit^{+}Lin^{-}Sca-1^{+}CD150^{+}CD48^{-}) isolated from the bone marrow of mice expressing CD45.2 were transplanted into lethally irradiated (9.8 Gy) congenic recipient mice (expressing CD45.1) along with 3 × 10^{5} Sca1-depleted bone marrow cells derived from an unirradiated recipient mouse. Peripheral blood of recipient mice was collected at 4, 8 and 28 weeks after transplantation. For *Lis1* chimera bone marrow transplants, 3 × 10^{5} whole bone marrow cells isolated from *Lis1* chimera mice (expressing CD45.2) were transplanted into lethally irradiated (9.8 Gy) recipient mice (expressing CD45.1) along with 3 × 10^{5} Sca1-depleted bone marrow cells derived from an unirradiated recipient mouse. Peripheral blood of recipient mice was collected at 16 weeks after transplantation.

Determining Numb inheritance. For experiments involving fixed cells, cells in late telophase or undergoing cytokinesis were identified by pronounced cytoplasmic cleft by brightfield or visualized by staining cells for alpha-tubulin plus the presence of dual nuclei using DAPI. ImageJ 1.46r was used to determine fluorescence intensity of pixels following staining for Numb. The fluorescence intensity of Numb was on average ~2.4-fold higher in the Numb^{high} daughter cell relative to the Numb^{low} daughter cell during an asymmetric division. On the basis of the data shown in **Figure 4b**, Numb expression was ~1.8-fold higher in progenitors than in HSCs, and, thus, incipient daughter cells that had at least a 1.8-fold difference in Numb expression were scored as showing asymmetric Numb inheritance. For live-imaging experiments, either KLS cells isolated from *Lis1*$^{f/f}$; *Rosa26-creER*/*Rosa26-creER* and *Lis1*$^{+/+}$; *Rosa26-creER*/*Rosa26-creER* mice or established wild-type or *Lis1*$^{-/-}$ blast-crisis CML lineage-negative cells were coinfected with mCherry–α-tubulin and Numb-CFP fusion constructs, and doubly infected cells were subsequently plated in methylcellulose medium (Methocult M3434, StemCell Technologies) and treated with 4-OH tamoxifen (Sigma). Please note that we used Numb-CFP specifically because it allowed clear detection of distinct levels of Numb. In contrast, expression of Numb-YFP led to highly saturated expression of YFP and did not allow easy differentiation of daughter cells with low and high Numb expression. Dividing cells identified in video replay were visualized in

spectrum color format (where red indicates pronounced α-tubulin expression and centrosome location) to readily identify the centrosomes. Using ImageJ 1.46r software, a line connecting the two centrosomes of a cell was drawn (line 1; dotted). Subsequently, an additional line (line 2; solid) was drawn perpendicular to line 1, which marked the cleavage furrow and partitioned the mother cell into incipient daughter cell 1 (D_1) and daughter cell 2 (D_2). Using the criteria described above and shown in **Figure 4b**, incipient daughter cells that showed at least a 1.8-fold difference in Numb expression were scored as having asymmetric Numb inheritance.

Analysis of spindle orientation and mitotic events. KLS cells were isolated and sorted from age- and sex-matched *Lis1*$^{f/f}$; *Rosa26-creER*/*Rosa26-creER* and *Lis1*$^{+/+}$; *Rosa26-creER*/*Rosa26-creER* mice and cultured overnight in X-Vivo 15 medium (Lonza) supplemented with 50 μM 2-mercaptoethanol, 10% FBS, SCF (100 ng/ml; R&D Systems) and thrombopoietin (20 ng/ml; R&D Systems). Cells were retrovirally infected with MSCV-H2B-GFP and mCherry–α-tubulin, harvested 48 h after infection and resorted for GFP$^+$mCherry$^+$ KLS cells. Sorted cells were either cultured in 96-well U-bottomed plates (BD Biosciences) for 48 h with 4-OH tamoxifen (Sigma) and subsequently placed on chambered coverslips (Lab-Tek II, Thermo Scientific) coated with 0.1 μg/μl Retronectin (Takara Bio) in the continual presence of 4-OH tamoxifen or plated in Iscove's modified medium–based methylcellulose medium (Methocult M3434, StemCell Technologies) supplemented with 4-OH tamoxifen. Images were acquired every 3–4 min with *xyzt* acquisition mode using an Axio Observer. Z1 microscope with the LSM 700 scanning module (Zeiss). Cultures were maintained at 37 °C and 5% CO_2 using a Heating Insert P Lab-Tek S1 with an Incubator PM S1 (Zeiss). Mitotic cells were identified in video replay. To measure spindle orientation, a concatenation of Z-stack images of each cell at every measured time point from the start of metaphase to early telophase was generated and displayed orthogonally using Zen 2010 software. Subsequently, the angle formed between the substratum plane (Retronectin base) and the virtual line passing through the spindle poles was measured using ImageJ 1.44. To quantify the duration of mitosis, the time between nuclear envelope breakdown and chromatin condensation until the beginning of telophase was determined. For chromosome counts, KLS cells were cultured in X-Vivo 15 medium (Lonza) supplemented with 50 μM 2-mercaptoethanol, 10% FBS, SCF (100 ng/ml; R&D Systems) and TPO (20 ng/ml; R&D Systems) for 48 h and then arrested in metaphase by a 2-h incubation with 100 ng/ml colcemid (KaryoMAX solution, Gibco). Cells were treated with hypotonic solution (0.56% KCl) for 15 min at 37 °C, fixed with 3:1 methanol:glacial acetic acid and spread on a slide to prepare metaphase spreads. Karyotyping was performed by Cell Line Genetics.

Generation and analysis of leukemic mice. KLS cells were isolated and sorted from age- and sex-matched *Lis1*$^{f/f}$; *Rosa26-creER*/*Rosa26-creER* and *Lis1*$^{+/+}$; *Rosa26-creER*/*Rosa26-creER* mice and cultured overnight in X-Vivo15 medium (Lonza) supplemented with 50 μM 2-mercaptoethanol, 10% FBS, SCF (100 ng/ml; R&D Systems) and TPO (20 ng/ml; R&D Systems). Cells were retrovirally infected with MSCV-BCR-ABL-IRES-YFP and MSCV-NUP98-HOXA9-IRES-GFP to generate myeloid blast-crisis-phase CML or with MSCV-MLL-AF9-IRES-GFP and MSCV-NRAS^{G12V}-IRES-YFP to generate *de novo* AML. Subsequently, cells were collected after 48 h of infection. Doubly infected cells (for blast-crisis CML experiments) or unsorted cells (for AML experiments) were transplanted retro-orbitally into cohorts of B6-CD45.1 mice. Before transplantation, for *de novo* AML transplants, infected cells regardless of donor genotype displayed similar infection efficiency. All recipients were sublethally (6–7 Gy) irradiated. For secondary blast-crisis CML transplantations, cells recovered from terminally ill primary recipients were sorted for lineage-negative (Lin$^-$), MSCV-BCR-ABL-IRES-YFP and MSCV-NUP98-HOXA9-IRES-GFP and transplanted into secondary recipients. Analysis of diseased mice was conducted as previously described[10].

Human leukemia samples and cell lines. Patient samples were obtained from Singapore General Hospital, the Fred Hutchinson Cancer Research Center, the Duke Adult Bone Marrow Transplant Clinic and Moores UCSD Cancer Center from institutional review board (IRB)-approved protocols with written informed consent in accordance with the Declaration of Helsinki. For colony-forming experiments, primary blast-crisis CML cells were resistant to imatinib, nilotinib and dasatinib, and primary AML cells harbored the *MLL-AF9* translocation. Leukemia cells were cultured in Iscove's modified Dulbecco medium (IMDM) supplemented with 10% FBS, 100 IU/ml penicillin and 100 μg/ml streptomycin, 55 μM 2-mercaptoethanol as well as SCF, interleukin (IL)-3, IL-6, FLT3L and TPO. For cell differentiation experiments, leukemia cells were cultured in IMDM supplemented with 20% BIT 9500 (StemCell Technologies), 2 mM L-glutamine, 100 IU/ml penicillin and 55 μM 2-mercaptoethanol as well as low-density lipoprotein (LDL), SCF and TPO. The human CML cell line K562 (American Type Culture Collection) was maintained in RPMI-1640 supplemented with 10% FBS, 100 IU/ml penicillin and 100 μg/ml streptomycin. The human AML cell line MV4-11 (American Type Culture Collection) was maintained in IMDM supplemented with 10% FBS, 100 IU/ml penicillin and 100 μg/ml streptomycin. For colony-forming assays, human cell lines or sorted hCD34$^+$ cells from primary patient samples were transduced with lentiviral shRNA (cloned in FG12-UbiC-GFP), and GFP-positive cells were sorted at 48 h and plated in complete methylcellulose medium (MethoCult Express, StemCell Technologies). All knockdown experiments were conducted with the construct shRNA-LIS1-(592) except those involving human primary CML cells, which were instead transduced with an alternative shRNA construct for *LIS1*, shRNA-LIS1-(1191). This construct represents an independent hairpin shRNA targeting *LIS1* that more effectively knocks down *LIS1* in these cells. Colony numbers were counted 10–14 d after plating.

Gene expression microarrays and data analysis. Control (*Lis1*$^{+/+}$; *Rosa26-creER*) or *Lis1*$^{f/f}$; *Rosa26-creER* mice were treated with tamoxifen for 5 consecutive days. Three days after the final tamoxifen administration, KLS cells were FACS sorted, and total cellular RNA was purified. RNA was amplified, labeled and hybridized onto Affymetrix GeneChip Mouse Genome 430 2.0 arrays. Raw hybridization data were collected (Asuragen). Expression-level data were normalized using a multiple-loess algorithm as previously described[48]. Probes whose expression levels exceed a threshold value in at least one sample were considered to have been detected. The threshold value was found by inspection of the distribution plots of $\log_2$ expression levels. Detected probes were sorted according to *q* value, the smallest false discovery rate (FDR)[49] at which the gene was called significant. An FDR of α was the expected fraction of false positives among all genes with $q \leq \alpha$. FDR was evaluated using Significance Analysis of Microarrays and its implementation in the official statistical package *samr*[50]. To prevent unwarranted variances, the percentile of s.d. values used for the exchangeability factor *s0* in the regularized *t* statistic was set to 50. The probe list, sorted by *q* value in ascending order, was translated into Entrez gene IDs and parsed so that when several different probes represented the same gene only the highest-ranking probe was kept for further analysis. The sorted list of genes was subjected to a non-parametric variant of Gene Set Enrichment Analysis (GSEA)[51], in which the *P* value of a gene set was defined as the minimal rank-order *P* value of a gene in the gene set[52] rather than the Kolmogorov-Smirnov statistic as in GSEA. Briefly, we let r_k be the *k*th-highest rank among a gene set of size *N*. The rank-order *P* value P_k of this gene was the probability that, among *N* randomly chosen ranks without replacement, the *k*th-highest rank would be at least r_k. The *P* value of a gene set was defined as the smallest of all P_k values. Finding the *P* value of a gene set of size *N* required calculation of *N* rank-order *P* values; however, there was no need to adjust *P* values for the number of genes tested, as the tests were highly statistically dependent. A Bonferroni adjustment of gene set *P* values for the number of gene sets tested was performed. Gene sets with adjusted *P* values ≤0.01 were reported. For the analysis of published stem cell signature sets[16–18,53–55], all detected genes in the *Lis1*$^{-/-}$ (*Lis1*$^{f/f}$; *creER* + tamoxifen) to control (*Lis1*$^{+/+}$; *creER* + tamoxifen) comparison were sorted according to *q* value as above, and GSEA for each signature gene set was performed. Each gene signature's *P* value was Bonferroni adjusted by a factor of 9 (number of signature gene sets tested). Heat maps were created using in-house hierarchical clustering software, and colors qualitatively correspond to fold changes.

PCR genotyping and RT-PCR analysis. For genotyping by PCR, the reaction mixture contained MangoMix (Bioline), genomic DNA and 0.5 μM of each primer. PCR conditions for genotyping were as follows: 3 min at 94 °C followed by 35 cycles of 94 °C for 30 s, 60 °C for 1 min and 72 °C for 1 min.

doi:10.1038/ng.2889

RNA was isolated using RNAqueous-Micro (Ambion) or RNeasy Mini kit (Qiagen). cDNA was prepared from equal amounts of RNA using Superscript II reverse transcriptase (Invitrogen). Quantitative RT-PCR was performed using iQ SYBR Green Supermix (Bio-Rad) on a CFX 96 C1000 Thermal Cycler (Bio-Rad). Results were normalized to the level of β2 microglobulin or TATA-binding protein. Mouse *Lis1* (*Pafah1b1*; Mm01253377_mH) mRNA levels were analyzed with TaqMan Gene Expression Assays. All primer sequences are listed in **Supplementary Table 2**.

Immunofluorescence staining. Cells were allowed to settle on coverslips coated with poly-L-lysine (BD Biosciences) at 37 °C, fixed with 4% paraformaldehyde (USB Corporation) or methanol, permeabilized with 1× Dako wash buffer (Dako) and blocked with 20% normal goat serum (Invitrogen) or donkey serum (Abcam) in 1× Dako wash buffer. Incubation with primary antibody was carried out overnight at 4 °C. The following primary antibodies were used: rabbit anti-Numb 1:50 or 1:100 (Abcam, ab14140), goat anti-LIS1 1:500 (Santa Cruz Biotechnology, sc7577), mouse anti–α-tubulin 1:200 (Abcam, ab7291), rat anti–α-tubulin 1:1,000 (Abcam, ab6161) and mouse anti–α-tubulin conjugate FITC 1:200 (Sigma, F2168). Incubation with secondary antibody was performed for 1 h at room temperature. DAPI (Molecular Probes) was used to detect DNA. Images were obtained with a Confocal Leica TCS SP5 II (Leica Microsystems) or an Axio Observer.Z1 microscope with the LSM 700 scanning module (Zeiss). ImageJ 1.46r software was used to determine fluorescence intensity.

Statistical analysis. Statistical analyses were carried out using GraphPad Prism software version 5.0a or 5.0d. Data are shown as mean ± s.e.m., and 'center values' are defined as the median. The χ^2 test was used to determine deviation from mendelian ratios. Two-tailed unpaired Student's *t* tests with Welch's correction when appropriate were used to determine statistical significance ($^*P < 0.05$, $^{**}P < 0.01$, $^{***}P < 0.001$, $^{****}P < 0.0001$).

45. Yang, Z.J. *et al.* Medulloblastoma can be initiated by deletion of *Patched* in lineage-restricted progenitors or stem cells. *Cancer Cell* **14**, 135–145 (2008).
46. Domen, J., Cheshier, S.H. & Weissman, I.L. The role of apoptosis in the regulation of hematopoietic stem cells: overexpression of Bcl-2 increases both their number and repopulation potential. *J. Exp. Med.* **191**, 253–264 (2000).
47. Qin, X.F., An, D.S., Chen, I.S. & Baltimore, D. Inhibiting HIV-1 infection in human T cells by lentiviral-mediated delivery of small interfering RNA against CCR5. *Proc. Natl. Acad. Sci. USA* **100**, 183–188 (2003).
48. Sásik, R., Woelk, C.H. & Corbeil, J. Microarray truths and consequences. *J. Mol. Endocrinol.* **33**, 1–9 (2004).
49. Benjamini, Y. & Hochberg, Y. Controlling the false discovery rate: a practical and powerful approach to multiple testing. *J. R. Stat. Soc. B* **57**, 289–300 (1995).
50. Tusher, V.G., Tibshirani, R. & Chu, G. Significance analysis of microarrays applied to the ionizing radiation response. *Proc. Natl. Acad. Sci. USA* **98**, 5116–5121 (2001).
51. Subramanian, A. *et al.* Gene set enrichment analysis: a knowledge-based approach for interpreting genome-wide expression profiles. *Proc. Natl. Acad. Sci. USA* **102**, 15545–15550 (2005).
52. Arnold, B.C., Balakrishnan, N. & Nagaraja, H.N. *A First Course in Order Statistics (Wiley Series in Probability and Statistics)* (John Wiley & Sons, New York, 1992).
53. Metzeler, K.H. *et al.* An 86-probe-set gene-expression signature predicts survival in cytogenetically normal acute myeloid leukemia. *Blood* **112**, 4193–4201 (2008).
54. Somervaille, T.C. *et al.* Hierarchical maintenance of MLL myeloid leukemia stem cells employs a transcriptional program shared with embryonic rather than adult stem cells. *Cell Stem Cell* **4**, 129–140 (2009).
55. Yagi, T. *et al.* Identification of a gene expression signature associated with pediatric AML prognosis. *Blood* **102**, 1849–1856 (2003).